



POLITECNICO
MILANO 1863

RE.PUBLIC@POLIMI

Research Publications at Politecnico di Milano

Post-Print

This is the accepted version of:

Á. Romero-Calvo, G. Cano Gómez, E. Castro-Hernández, F. Maggi
Free and Forced Oscillations of Magnetic Liquids Under Low-Gravity Conditions
Journal of Applied Mechanics - Transactions of the ASME, Vol. 87, N. 2, 2020,
021010 (9 pages)
doi: 10.1115/1.4045620

The final publication is available at <https://doi.org/10.1115/1.4045620>

Access to the published version may require subscription.

When citing this work, cite the original published paper.

© 2020 by ASME. This manuscript version is made available under the CC-BY 4.0 license
<http://creativecommons.org/licenses/by/4.0/>

Permanent link to this version

<http://hdl.handle.net/11311/1129359>



American Society of
Mechanical Engineers

ASME Accepted Manuscript Repository

Institutional Repository Cover Sheet

Filippo

Maggi

First

Last

ASME Paper Title: Free and Forced Oscillations of Magnetic Liquids Under Low-Gravity Conditions

Authors: Romero-Calvo, Álvaro; Cano Gómez, Gabriel; Castro-Hernández, Elena; Maggi, Filippo

ASME Journal Title: Journal of Applied Mechanics - Transactions of the ASME

Volume/Issue 87/2 Date of Publication (VOR* Online) Dec 19th, 2019

ASME Digital Collection URL: <https://asmedigitalcollection.asme.org/appliedmechanics/article/doi/10.1115/1.4045620>
e-and-Forced-Oscillations-of-Magnetic-Liquids

DOI: 10.1115/1.4045620

*VOR (version of record)

Free and forced oscillations of magnetic liquids under low-gravity conditions

Álvaro Romero-Calvo¹, Gabriel Cano Gómez², Elena Castro-Hernández³, and Filippo Maggi¹

¹Space Propulsion Laboratory, Department of Aerospace Science and Technology, Politecnico di Milano, Via Giuseppe La Masa, 34, 20156, Milan, Italy

²Departamento de Física Aplicada III, Universidad de Sevilla, Avenida de los Descubrimientos s/n, 41092, Sevilla, Spain

³Área de Mecánica de Fluidos, Dep. Ingeniería Aeroespacial y Mecánica de Fluidos, Universidad de Sevilla, Avenida de los Descubrimientos s/n, 41092, Sevilla, Spain

The sloshing of liquids in microgravity is a relevant problem of applied mechanics with important implications for spacecraft design. A magnetic settling force may be used to avoid the highly non-linear dynamics that characterize these systems. However, this approach is still largely unexplored. This paper presents a quasi-analytical low-gravity sloshing model for magnetic liquids under the action of external inhomogeneous magnetic fields. The problems of free and forced oscillations are solved for axisymmetric geometries and loads by assuming a linear behavior. The model may be of particular interest for the development of magnetic sloshing damping devices in space, whose behavior can be easily predicted and quantified with standard mechanical analogies.

Nomenclature

| | |
|----------------|---|
| \mathbf{A} | Magnetic vector potential |
| \mathbf{A}_0 | Dipole term of \mathbf{A} |
| A_n | Forced problem coefficients for ϕ |
| a | Axisymmetric tank radius at the contour of the meniscus |
| a_{ip} | Modal coefficients used by $\bar{\Phi}_i$, $\bar{\zeta}_i$ and $\bar{\xi}_i$ |
| β | Arbitrary time constant of Bernoulli's equation |
| \mathbf{B} | Magnetic flux density |
| B_n | Forced problem coefficients for h |
| Bo | Bond number |
| Bo_{mag} | Magnetic Bond number |
| χ | Magnetic susceptibility |
| C | Dynamic contour |
| C' | Meniscus contour |
| $C_i^{(n)}$ | Modal coefficients used by $\Phi^{(n)}$, $\mathcal{H}^{(n)}$ and $G^{(n)}$ |
| F | Dimensionless f |
| f | Relative height between meniscus and vertex |
| Γ | Dimensionless γ |
| γ | Surface hysteresis parameter |
| G | Wall boundary condition function |
| $G^{(n)}$ | Eigenfunctions of G |
| g | Inertial acceleration |
| g_0 | Gravity acceleration at ground level |
| \mathcal{H} | Dimensionless h |

| | |
|----------------------|---|
| $\mathcal{H}^{(n)}$ | Eigenfunctions of \mathcal{H} |
| \mathbf{H} | Magnetic field |
| \mathbf{H}_0 | Applied magnetic field |
| h | Relative height between meniscus and dynamic liquid surface |
| h_m | Height of the cylindrical magnet |
| I | Variational principle |
| K | Curvature of the liquid surface |
| λ | Equilibrium free surface parameter |
| \bar{L}_{ij} | Matrix from Eq. (29) |
| \bar{L}_{ij}^{mag} | Matrix from Eq. (29) |
| μ_0 | Magnetic permeability of free space |
| \mathbf{M} | Magnetization field |
| M_n | Magnetization component normal to the fluid surface |
| ν | Kinematic viscosity |
| N | Size of the set of admissible functions |
| \mathbf{n} | Unitary external vector normal to the fluid surface |
| Ω | Dimensionless ω |
| ω | Circular frequency of the surface wave |
| Ω_n | Dimensionless ω_n |
| ω_n | Modal circular frequency of the surface wave |
| O | Vertex of the meniscus |
| p | Thermodynamic pressure |
| p^* | Composite pressure |
| p_c | Capillary pressure |
| p_g | Filling gas pressure |
| p_n | Magnetic normal traction |
| p_0 | Thermodynamic pressure at the vertex of the meniscus |
| Φ | Dimensionless ϕ |
| $\Phi^{(n)}$ | Eigenfunctions of Φ |
| $\bar{\Phi}_i$ | Admissible functions of $\Phi^{(n)}$ |
| φ | Liquid velocity potential |
| ϕ_0 | Rigid-body liquid velocity potential |
| ϕ | Perturbed liquid velocity potential |
| ψ | Magnetic force potential |
| $\bar{\psi}$ | Dimensionless magnetic term at the meniscus |
| Q_{ij} | Matrix from Eq. (29) |
| ρ | Liquid density |
| R_{ij} | Matrix from Eq. (29) |
| r_e | External radius of the cylindrical magnet |
| r_i | Internal radius of the cylindrical magnet |

| | |
|---|---|
| σ | Surface tension |
| \mathcal{S} | Dimensionless s |
| S | Dynamic fluid surface |
| S' | Meniscus surface |
| s | Curvilinear coordinate along the meniscus |
| $\bar{\theta}_c$ | Surface contact angle referred to the vertical |
| θ_c | Surface contact angle |
| ϑ_p | Primitive functions of $\bar{\Phi}_i$ |
| V | Liquid volume |
| \mathbf{v} | Liquid velocity |
| v | Specific volume |
| W | Walls of the container |
| \bar{w} | Relative height between dynamic liquid surface and vertex for a particular surface point |
| w | Relative height between dynamic liquid surface and vertex |
| $\bar{\xi}_i$ | Admissible functions of $G^{(n)}$ |
| ξ_p | Primitive functions of $\bar{\xi}_i$ |
| x | Lateral displacement of the container |
| Z | Dimensionless z |
| $\bar{\zeta}_i$ | Admissible functions of $\mathcal{H}^{(n)}$ |
| ζ_p | Primitive functions of $\bar{\zeta}_i$ |
| $\{r, \theta, z\}$ | Cylindrical coordinates of the system $\{\mathbf{u}_r, \mathbf{u}_\theta, \mathbf{u}_z\}$ |
| $\{\mathbf{u}_r, \mathbf{u}_\theta, \mathbf{u}_z\}$ | Cylindrical reference system centered at the vertex of the meniscus |

1 Introduction

The term sloshing refers to the forced movement of liquids in partially filled tanks [1]. Propellant sloshing has been a major concern for space engineers since the beginning of the space era. During launch, it can result in the partial or total loss of control of the spacecraft [2]. In a low-gravity environment, the liquid tends to adopt a random position inside the tank and mixes with pressurizing gas bubbles. This results in a complicated propellant management system design, often increasing the inert mass of the vehicle [1].

Low-gravity sloshing is characterized by the dominant role of surface tension, that produces a curved equilibrium free surface (or meniscus) and a complex interaction with the walls of the vessel that contains the liquid. The first solution of the low-gravity free surface oscillation problem was given in 1964 by Satterlee and Reynolds for cylindrical containers [3]. In the context of the Space Race, a significant effort was made to study low-gravity sloshing in cylindrical [3–9], spheroidal [8, 10, 11] or axisymmetric [12–15] tanks. A non-extensive list of modern works includes numerical models for cryogenics [16, 17], coupled non-linear implementations [18] or Computational Fluid Dynamics (CFD) simulations [19]. Analytical solutions of the free and forced oscillations problem were found by Utsumi [20–23].

Different active and passive strategies have been traditionally employed to mitigate liquid sloshing in microgravity. *Active* approaches settle the propellant by imposing an adequate inertial force with a set of thrusters. *Passive* techniques make use of surface tension or membranes to hold the liquid at a certain position and reduce the effect of random accelerations. The resulting technical implementations,

named *Propellant Management Devices*, are currently used to grant adequate liquid propellant feeding in case of in-orbit ignition of chemical propulsion units [24].

Since the absence of a settling volume force is the main characteristic of low-gravity sloshing, the problem could be attacked by reproducing the force of gravity with electromagnetic fields if the liquid can answer to such stimulus. The use of *dielectrophoresis*, a phenomenon on which a force is exerted on dielectric particles in the presence of a non-uniform electric field, was explored by the US Air Force with dielectric propellants in 1963 [25]. The study unveiled a high risk of arcing inside the tanks and highlighted the need of large, heavy and noisy power sources. Approaches exploring *Magnetic Positive Positioning* have also been suggested to exploit the inherent magnetic properties of paramagnetic (oxygen) and diamagnetic (hydrogen) liquids. Relatively recent studies employed numerical simulations and microgravity experiments to validate this concept [26, 27].

Ferrofluids are colloidal suspensions of magnetic nanoparticles treated with a surfactant to prevent from agglomeration. As a result, they exhibit high magnetic susceptibility. Their invention is attributed to Steve Papell, who in 1963 proposed to “provide an artificially imposed gravity environment” with ferrofluid-based magnetic propellants [28]. The basic equations governing the dynamics of ferrofluids were presented in 1964 by Neuringer and Rosensweig [29], giving rise to the field of Ferrohydrodynamics [30]. Although since then ferrofluids have found numerous applications on Earth, works addressing their original purpose are scarce. A rare exception is the NASA Magnetically Actuated Propellant Orientation (MAPO) experiment, that studied the magnetic positioning of liquid oxygen and validated a custom CFD model with a series of parabolic flight experiments with ferrofluids [31]. Subsequent publications presented numerical models to study and generalize the measurements for space applications [32–34].

One of the main drawbacks of magnetic sloshing control is the rapid decay of magnetic fields, that limits its applicability to small and compact tanks. In this context, the increasing number of propelled microsatellites may benefit from this technology since a direct control of liquid sloshing could be achieved with small low-cost magnets. Once the liquid is positioned, magnetic fields could also be used to tune the natural frequencies and damping ratios of the system. This approach has been adopted for terrestrial applications, such as Tuned Magnetic Liquid Dampers [35, 36]. On-ground research exploring axisymmetric sloshing [37, 38], the frequency shifts due to the magnetic interaction [39], two-layer sloshing [40] or the swirling phenomenon [41], among others, has been carried out in the past with notable results. The sloshing of ferrofluids in low-gravity was indirectly studied in 1972 with a focus on gravity compensation techniques [42].

This work addresses the free and forced oscillations of magnetic liquids in axisymmetric containers when subjected to an external inhomogeneous magnetic field in microgravity. A ferrohydrodynamic model is developed to predict the natural frequencies and modal shapes of the system and a

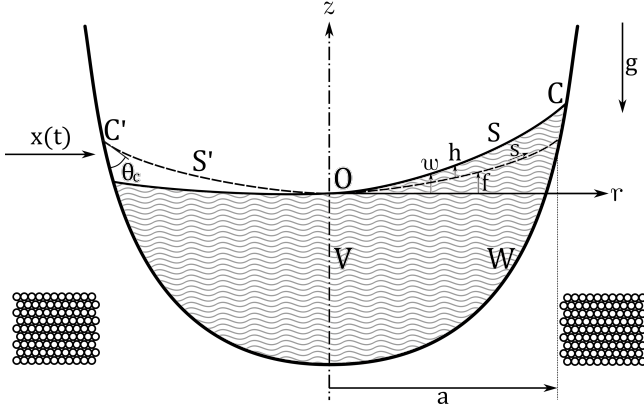


Fig. 1: Geometry of the system under analysis, composed by a magnetic liquid that fills a container in microgravity while subjected to an external magnetic field. S' and C' refer to the meniscus surface and contour, while S and C are the dynamic fluid surface and contour, respectively. O denotes the vertex of the meniscus, W is the vessel wall and V denotes the fluid volume.

case of application is presented. Unlike non-magnetic low-gravity sloshing, the presence of a restoring force ensures that the hypothesis of small oscillations (linear sloshing) is satisfied in a wide range of operation.

2 Problem formulation

The system to be modeled is represented in Fig. 1. A volume V of a magnetic liquid fills an upright axisymmetric tank with radius a at the meniscus contour. The liquid is incompressible, Newtonian and is characterized by a density ρ , specific volume $v = \rho^{-1}$, kinematic viscosity ν , surface tension σ and magnetization curve $M(H)$. H and M are respectively the modules of the magnetic field \mathbf{H} and magnetization field \mathbf{M} , which are assumed to be collinear. The liquid meets the container wall with a contact angle θ_c . An applied inhomogeneous axisymmetric magnetic field \mathbf{H}_0 is imposed by an external source (e.g. a coil located at the base of the container). The inertial acceleration g along the z axis is also considered. A non-reactive gas at pressure p_g fills the free space. In the figure, s is a curvilinear coordinate along the meniscus with origin in the vertex O and the relative heights are given by w (fluid surface - vertex), f (meniscus - vertex) and h (fluid surface - meniscus). The container is subjected to a lateral displacement $x(t)$. The meniscus is represented by a dashed line and the dynamic fluid surface is given by a solid line. The model here presented extends the works by Satterlee & Reynolds [3] and Yeh [12] by considering the magnetic interaction and the axisymmetric oscillations case.

2.1 Nonlinear formulation

A cylindrical reference system $\{\mathbf{u}_r, \mathbf{u}_\theta, \mathbf{u}_z\}$, centered at the vertex of the meniscus, is subsequently considered. If an irrotational flow field is assumed, there exists a potential ϕ such that

$$\mathbf{v} = -\nabla\phi = -\phi_r\mathbf{u}_r - \frac{1}{r}\phi_\theta\mathbf{u}_\theta - \phi_z\mathbf{u}_z, \quad (1)$$

being \mathbf{v} the flow velocity with the subindices denoting the derivative. The velocity potential satisfies Laplace's equation

$$\nabla^2\phi = \phi_{rr} + \frac{\phi_r}{r} + \frac{\phi_{\theta\theta}}{r^2} + \phi_{zz} = 0 \text{ in } V, \quad (2)$$

subjected to the non-penetration wall boundary condition

$$\phi_r = -\dot{x}\cos\theta, \quad \phi_\theta/r = \dot{x}\sin\theta, \quad \phi_z = 0 \text{ on } W. \quad (3)$$

An additional boundary condition at the free surface is given by the unsteady ferrohydrodynamic Bernoulli's equation, which for an isothermal system with collinear magnetization field \mathbf{M} adopts the form [30, 43]

$$-\dot{\phi} + \frac{\|\mathbf{v}\|^2}{2} + \frac{p^*}{\rho} + gw - \frac{\psi}{\rho} + \dot{x}\cos\theta\phi_r - \dot{x}\sin\theta\frac{\phi_\theta}{r} = \beta(t) \text{ on } S, \quad (4)$$

where g is the inertial acceleration, ψ is the magnetic force potential, $\beta(t)$ is an arbitrary function of time and p^* is the composite pressure, defined as [30]

$$p^* = p(\rho, T) + \mu_0 \int_0^H \left(v \frac{\partial M}{\partial v} \right)_{H, T} dH + \mu_0 \int_0^H M(H) dH, \quad (5)$$

with the first, second and third terms being named thermodynamic, *magnetostrictive* and *fluid-magnetic* pressure, respectively. For magnetically diluted systems $M \sim \rho$, where ρ is represented by the magnetic particles concentration for the case of ferrofluids. Under this additional assumption, both pressure-like components are approximately compensated, and hence $p^* \approx p(\rho, T)$ [30].

The *canonical* magnetic force per unit volume is given by $\mu_0\mathbf{M}\nabla\mathbf{H}$, with $\mu_0 = 4\pi \cdot 10^{-7} \text{N/A}^2$ being the permeability of free space [30]. It can be shown that, for an isothermal fluid, this force derives from the potential [29]

$$\Psi = \mu_0 \int_0^H M(H) dH. \quad (6)$$

Due to the discontinuity of the Maxwell stress tensor at the magnetic liquid interface, the ferrohydrodynamic boundary condition in the absence of viscous forces becomes

$$p^* = p_g - p_c - p_n \text{ on } S, \quad (7)$$

where $p_n = \mu_0 M_n^2/2$ is the *magnetic normal traction*, M_n is the magnetization component normal to the fluid surface, and p_c is the *capillary pressure*. The last is defined by the Laplace-Young equation $p_c = \sigma K$, where

$$K = \frac{1}{r} \frac{\partial}{\partial r} \left[\frac{r w_r}{\sqrt{1 + w_r^2 + \frac{1}{r^2} w_\theta^2}} \right] + \frac{1}{r^2} \frac{\partial}{\partial \theta} \left[\frac{w_\theta}{\sqrt{1 + w_r^2 + \frac{1}{r^2} w_\theta^2}} \right] \quad (8)$$

is the curvature of the surface [1]. Since at Eq. (4) only the spatial derivatives of the velocity potential have a physical meaning (e.g. Eq. (1)), any function of time can be added to φ whenever it is convenient. From a physical viewpoint, the absolute value of p remains undetermined under the incompressible flow assumption [43]. The integration constant $\beta(t)$ can be then absorbed into the definition of φ . By arbitrarily selecting $\beta(t) = p_g/\rho$, the dynamic interface condition is obtained

$$\dot{\varphi} - \frac{1}{2} \left(\varphi_r^2 + \frac{1}{r^2} \varphi_\theta^2 + \varphi_z^2 \right) + \frac{\sigma}{\rho} K - g w + \frac{\Psi}{\rho} + \frac{\mu_0 M_n^2}{2\rho} - \dot{x} \cos \theta \varphi_r + \dot{x} \sin \theta \frac{\varphi_\theta}{r} = 0 \text{ on } S. \quad (9)$$

In an inertial reference system, the vertical displacement \bar{w} of a surface point lying at $(\bar{r}, \bar{\theta})$ in the interface $z = w(r, \theta, t)$ is given by

$$\frac{d\bar{w}}{dt} = \dot{w} + w_r \frac{d\bar{r}}{dt} + w_\theta \frac{d\bar{\theta}}{dt} \text{ on } S. \quad (10)$$

If the velocity components relative to the tank $d\bar{w}/dt$, $d\bar{r}/dt$ and $d\bar{\theta}/dt$ are expressed as a function of the potential given by Eq. (1), the kinematic interface condition that relates the last with the shape of the free surface is

$$\dot{w} = -\varphi_z + w_r (\varphi_r + \dot{x} \cos \theta) + \frac{w_\theta}{r^2} (\varphi_\theta - \dot{x} r \sin \theta) \text{ on } S. \quad (11)$$

The continuity equation given by Eq. (2), together with the kinematic relation in Eq. (11) and the boundary conditions at Eq. (3) and Eq. (9), conform the problem to be solved after imposing the contact angle at the wall (θ_c) and a contact hysteresis parameter that will be described later in the text.

2.2 Equilibrium free surface shape

Due to the axisymmetry of geometry and loads, the static equilibrium surface of the fluid (S') is also axisymmetric. Its shape can be easily determined from the balance of

vertical forces in a circular crown of inner radius r and infinitesimal width dr along the surface [24]. This results in the following set of dimensionless differential equations

$$\frac{d}{dS} \left(R \frac{dF}{dS} \right) = R \frac{dR}{dS} [\lambda + BoF - \bar{\Psi}(R)], \quad (12a)$$

$$\frac{dF}{dS} \frac{d^2 F}{dS^2} + \frac{dR}{dS} \frac{d^2 R}{dS^2} = 0, \quad (12b)$$

and boundary conditions

$$R(0) = F(0) = \frac{dF(0)}{dS} = 0, \quad \frac{dR(0)}{dS} = 1, \quad (12c)$$

$$\frac{dF(1)}{dR} = \tan \left(\frac{\pi}{2} - \bar{\theta}_c \right), \quad (12d)$$

where $R = r/a$, $F = f/a$, $S = s/a$, $Bo = \rho g a^2 / \sigma$ is the Bond number, $\lambda = a(p_g - p_0) / \sigma$, being p_0 the liquid pressure at the free surface vertex, $\bar{\Psi}$ includes the magnetic potential and magnetic normal traction through

$$\bar{\Psi}(R) = \frac{a\mu_0}{\sigma} \left[\int_{H(0,0)}^{H(R,F(R))} M(H) dH + \frac{M_n^2}{2} \right]_{F(R)}, \quad (13)$$

and the static contact angle with respect to the vertical $\bar{\theta}_c$ is given by

$$\bar{\theta}_c = \theta_c + \frac{\pi}{2} - \arctan \left(\frac{dW}{dr} \Big|_{C'} \right). \quad (14)$$

A numerical solution can be easily computed by (1) setting an initial vertex position, (2) calculating the value of λ iteratively in order to satisfy the contact angle condition given by Eq. (12d), (3) solving the system with an ODE solver, and (4) obtaining the new height of the vertex through volume conservation. The procedure is repeated until the vertex height converges with a prescribed relative variation. When non-trivial magnetic setups are involved, a FEM simulation must be included in the loop.

2.3 Linear equations

The dynamic and kinematic conditions at Eq. (9) and Eq. (11) are highly nonlinear. The standard analytical procedure overcomes this difficulty by linearizing the problem and restricting the analysis to small oscillations. If the wave position is expressed as the sum of the static equilibrium solution and a small perturbation

$$w(r, \theta, t) = f(r) + h(r, \theta, t), \quad (15)$$

it will be possible to express the system of equations and boundary conditions as a Taylor's series expansion around the equilibrium surface S' . If second-order terms are neglected, the boundary-value problem becomes

$$\nabla^2 \varphi = 0 \text{ in } V, \quad (16a)$$

$$\varphi_r = -\dot{x} \cos \theta, \quad \varphi_\theta / r = \dot{x} \sin \theta, \quad \varphi_z = 0 \text{ on } W. \quad (16b)$$

$$\begin{aligned} \varphi + \frac{\sigma}{\rho} \left\{ \frac{1}{r} \frac{\partial}{\partial r} \left[\frac{r h_r}{(1 + f_r^2)^{3/2}} \right] \right. \\ \left. + \frac{1}{r^2} \frac{\partial}{\partial \theta} \left[\frac{h_\theta}{\sqrt{1 + f_r^2}} \right] \right\} \\ - \left[g - \frac{\mu_0}{\rho} \left(M \frac{\partial H}{\partial z} + M_n \frac{\partial M_n}{\partial z} \right) \right] h = 0 \text{ on } S', \end{aligned} \quad (16c)$$

$$\dot{h} = -\varphi_z + f_r(\varphi_r + \dot{x} \cos \theta) \text{ on } S', \quad (16d)$$

$$h_r = \gamma h \text{ on } C', \quad (16e)$$

Equation 16e assumes that the slope of the perturbation field at the wall is related to the magnitude of the perturbation at the same point through the parameter γ . The *free-edge condition* is characterized by $\gamma = 0$, while the *stuck-edge condition* is associated with $\gamma \rightarrow \infty$ [12]. This assumption is far from being rock-solid, and has indeed motivated a strong debate in the past. It has been suggested that the contact angle hysteresis condition depends not only on the position of the wave but also on its *velocity* [4] or the state of the wall [7]. In the absence of a clear criteria, some studies assume the free-edge condition or intermediate approaches, generally obtaining a reasonable agreement with experimental data [10].

The only difference between the previous formulation and the classical problem without magnetic interactions is given by the magnetic term in Eq. (16c). The effective gravity acceleration includes both inertial and magnetic components and is given by

$$g^*(r) = g - \frac{\mu_0}{\rho} \left(M \frac{\partial H}{\partial z} + M_n \frac{\partial M_n}{\partial z} \right)_S, \quad (17)$$

where it can be observed that the magnetic contribution is a function of the radius. The magnitude and relative importance of the magnetic terms depend on the magnetic configuration and gravity level of the system under analysis. In particular, the magnetic component will be more significant in the absence of gravity.

The magnetic field modifies the effective gravity acceleration of the system and shifts its natural frequencies, as

reported in normal-gravity works [35, 44]. If the magnetic term was approximately constant in R , like in the case of a linear magnetic field and a flat surface, the problem would be equivalent to the non-magnetic system [42]. In this analysis, however, an inhomogeneous magnetic field is being considered.

2.4 Extraction of tank motion

The potential φ has been referred to an inertial reference system. In order to analyze the movement of the free surface in the tank reference frame, it would be convenient to split this potential into rigid body (ϕ_0) and perturbed (ϕ) components, so that

$$\varphi = \phi_0 + \phi, \quad \phi_0 = -\dot{x} r \cos \theta. \quad (18)$$

The boundary-value problem can be then expressed as a function of the perturbed potential and becomes

$$\nabla^2 \phi = 0 \text{ in } V, \quad (19a)$$

$$\phi_n = 0 \text{ on } W, \quad (19b)$$

$$\begin{aligned} \phi + \frac{\sigma}{\rho} \left\{ \frac{1}{r} \frac{\partial}{\partial r} \left[\frac{r h_r}{(1 + f_r^2)^{3/2}} \right] \right. \\ \left. + \frac{1}{r^2} \frac{\partial}{\partial \theta} \left[\frac{h_\theta}{\sqrt{1 + f_r^2}} \right] \right\} - \left[g \right. \\ \left. - \frac{\mu_0}{\rho} \left(M \frac{\partial H}{\partial z} + M_n \frac{\partial M_n}{\partial z} \right) \right] h = \ddot{x} r \cos \theta \text{ on } S', \end{aligned} \quad (19c)$$

$$\dot{h} = -\phi_z + \phi_r f_r \text{ on } S', \quad (19d)$$

$$h_r = \gamma h \text{ on } C'. \quad (19e)$$

3 Free oscillations problem

3.1 Dimensionless linear equations

In [3, 12] it is proposed to split the potentials ϕ and h into spatial and temporary components, the second being a cyclic function of time with a circular frequency ω . The resulting dimensionless boundary-value problem is

$$\nabla^2 \Phi = 0 \text{ in } V, \quad (20a)$$

$$\frac{\partial \Phi}{\partial n} = 0 \text{ on } W, \quad (20b)$$

$$\begin{aligned} \Omega^2 \Phi - [Bo + Bo_{mag}(R)] \mathcal{H} & \mathcal{H}_R = \Gamma \mathcal{H} \text{ on } C', \quad (22e) \\ + \frac{1}{R} \frac{\partial}{\partial R} \left[\frac{R \mathcal{H}_R}{(1 + F_R^2)^{3/2}} \right] & \\ + \frac{1}{R^2} \frac{\partial}{\partial \theta} \left[\frac{\mathcal{H}_\theta}{\sqrt{1 + F_R^2}} \right] = 0 \text{ on } S', & \quad (20c) \end{aligned}$$

$$\mathcal{H} = \Phi_Z - \Phi_R F_R \text{ on } S', \quad (20d)$$

$$\mathcal{H}_R = \Gamma \mathcal{H} \text{ on } C', \quad (20e)$$

where $R = r/a$, $Z = z/a$, $F = f/a$, $\phi(R, \theta, Z, t) = \sqrt{g_0 a^3} \Phi(R, \theta, Z) \sin(\omega t)$, $h(R, \theta, t) = \sqrt{a g_0 / \omega^2} \mathcal{H}(R, \theta) \cos(\omega t)$, $\Omega^2 = \rho a^3 \omega^2 / \sigma$, $\Gamma = a \gamma$ and g_0 is the acceleration of gravity at ground level [1]. The *Magnetic Bond Number* has been defined as

$$Bo_{mag}(R) = -\frac{\mu_0 a^2}{\sigma} \left(M \frac{\partial H}{\partial z} + M_n \frac{\partial M_n}{\partial z} \right)_{F(R)}, \quad (21)$$

and accounts for the effects of the external magnetic field on the liquid.

3.2 Variational formulation

By following the procedure described in [3, 12], it is possible to develop a variational principle equivalent to Eq. (20b) and Eq. (20c) as

$$\begin{aligned} I = \iint_{S'} \left[\frac{\mathcal{H}_R^2}{(1 + F_R^2)^{3/2}} + \frac{1}{R^2} \frac{\mathcal{H}_\theta^2}{(1 + F_R^2)^{1/2}} \right. & \\ \left. + (Bo + Bo_{mag}(R)) \mathcal{H}^2 - \Omega^2 \Phi \mathcal{H} \right] R dR d\theta & \\ - \Omega^2 \iint_W \Phi G R dR d\theta - \Gamma \int_{C'} \left[\frac{\mathcal{H}^2}{(1 + F_R^2)^{3/2}} \right]_{R=1} d\theta & \\ = \text{extremum,} & \quad (22a) \end{aligned}$$

subjected to

$$\nabla^2 \Phi = 0 \text{ in } V, \quad (22b)$$

$$\mathcal{H} = \Phi_Z - F_R \Phi_R \text{ on } S', \quad (22c)$$

$$G = \Phi_Z - W_R \Phi_R \text{ on } W, \quad (22d)$$

where G and its associated terms arise from the application of the wall boundary condition given by Eq. (20b) as detailed in [12]. The obtention of this variational formulation follows the procedure described in [12, 45].

3.3 Ritz method

The previous set of equations can only be analytically solved for simplified configurations in the absence of magnetic fields, like the case of a cylindrical container with flat bottom and flat fluid surface ($\theta_c = 90^\circ$) [3]. For other physical systems, Ritz approximations [1, 12] or finite differences approaches [5, 6] have been proposed to approximate the eigenfunctions of the problem. The basic formulation of the first approach is subsequently developed based on [3, 12].

By following Ritz's method, the eigenfunctions $\Phi^{(n)}$ can be approximated as the linear combination of admissible functions $\bar{\Phi}_i(R, \theta, Z)$ that satisfy the boundary conditions of the problem described by Eq. (22b) to Eq. (22e). This results in

$$\Phi^{(n)} = \sum_{i=1}^N C_i^{(n)} \bar{\Phi}_i \quad (n=1, \dots, N), \quad (23)$$

where N is the size of the set of admissible functions. In the same way, the eigenfunctions $\mathcal{H}_i^{(n)}$ and $G^{(n)}$ are approximated by $\bar{\zeta}_i(R, \theta)$ and $\bar{\xi}_i(R, \theta)$ through

$$\mathcal{H}^{(n)} = \sum_{i=1}^N C_i^{(n)} \bar{\zeta}_i, \quad (24)$$

$$G^{(n)} = \sum_{i=1}^N C_i^{(n)} \bar{\xi}_i. \quad (25)$$

The sets of admissible functions are linked through Eq. (22c) and Eq. (22d). If $\Phi^{(n)}$, $\mathcal{H}^{(n)}$ and $G^{(n)}$ are continuous functions of $C_i^{(n)}$, the extremum condition represented by Eq. (22a) requires that

$$\frac{\partial I}{\partial C_i^{(n)}} = 0, \quad (i=1, 2, \dots, N), \quad (26)$$

which results in the system of equations

$$\sum_{i=1}^N C_i^{(n)} (R_{ij} + Bo \bar{L}_{ij} + \bar{L}_{ij}^{mag} - \Omega_n^2 Q_{ij}) = 0, \quad (j=1, 2, \dots, N), \quad (27)$$

being

$$R_{ij} = \iint_F \left[\frac{\bar{\zeta}_{iR}\bar{\zeta}_{jR}}{(1+F_R^2)^{3/2}} + \frac{n^2\bar{\zeta}_i\bar{\zeta}_j}{R^2(1+F_R^2)^{1/2}} \right] RdRd\theta - \Gamma \int_0^{2\pi} \left[\frac{\bar{\zeta}_i\bar{\zeta}_j}{(1+F_R^2)^{3/2}} \right]_{R=1} d\theta, \quad (28a)$$

$$\bar{L}_{ij} = \iint_F \bar{\zeta}_i\bar{\zeta}_j RdRd\theta, \quad (28b)$$

$$\bar{L}_{ij}^{mag} = \iint_F Bo_{mag}(R)\bar{\zeta}_i\bar{\zeta}_j RdRd\theta, \quad (28c)$$

$$Q_{ij} = \frac{1}{2} \iint_F (\bar{\Phi}_i\bar{\zeta}_j + \bar{\Phi}_j\bar{\zeta}_i) RdRd\theta + \frac{1}{2} \iint_F (\bar{\Phi}_i\bar{\xi}_j + \bar{\Phi}_j\bar{\xi}_i) RdRd\theta. \quad (28d)$$

The system has a nontrivial solution only when its determinant is zero. The eigenvalues Ω_n^2 , and therefore the corresponding modal circular frequencies ω_n , are then computed by means of the characteristic equation

$$\|R_{ij} + BoL_{ij} + L_{ij}^{mag} - \Omega^2 Q_{ij}\| = 0. \quad (29)$$

Once solved, the eigenfunctions of the problem are obtained from Eq. (23) to Eq. (25).

3.4 Forced lateral oscillations and mechanical analogies

In order to solve the forced lateral oscillations case, a modal solution for the linearized boundary-value problem given by Eq. (19) is built from the eigenmodes $\Phi^{(n)}$ and $\mathcal{H}^{(n)}$. This solution is expressed as

$$\phi = \sum_{n=1}^N A_n(t)\Phi^{(n)}, \quad h = \sum_{n=1}^N B_n(t)\mathcal{H}^{(n)}, \quad (30)$$

where the modal coordinates $A_n(t)$ and $B_n(t)$ are computed from their corresponding modal equations. The reader is referred to [12] for a full description of this procedure.

Since the modal equations are linear, the forced sloshing problem can be assimilated as the superposition of several linear oscillators. These are usually assumed to be a series of spring-mass systems on which a linear damper is included *a posteriori*. The employment of a mechanical analogy simplifies the integration of the sloshing problem into the equations of motion of the vehicle. In the case here analyzed, an additional magnetic pressure should be considered. However, in virtue of Newton's action-reaction principle, if the magnetic source is rigidly coupled to the tank then the distribution of

magnetic pressures cannot produce torque in the assembly. That is, non-magnetic mechanical analogies can be extended for the magnetic case by simply employing the new magnetic eigenmodes $\Phi^{(n)}$ and $\mathcal{H}^{(n)}$ with their corresponding eigenfrequencies. Some possibilities are the models developed by Dodge [46] or Utsumi [23].

3.5 Selection of admissible and primitive functions

The set of admissible functions for Φ , \mathcal{H} and G , related through Eq. (22c) and Eq. (22d), satisfy by definition Eq. (22b) to Eq. (22e) and form truncated series that approximate the eigenfunctions of the problem. A set of primitives should be previously defined as [3]

$$\vartheta_p = J_n(k_p R) \cos(m\theta) e^{k_p Z} \quad (p=1, \dots, N, N+1), \quad (31a)$$

$$\zeta_p = (\vartheta_{pZ} - F_R \vartheta_{pR})_{Z=F(R)}, \quad (31b)$$

$$\xi_p = (\vartheta_{pZ} - W_R \vartheta_{pR})_{Z=W(R)}, \quad (31c)$$

with k_p being the roots of the equation

$$\left[\frac{d}{dR} J_n(k_i R) \right]_{R=1} = 0, \quad (32)$$

where J_n is the Bessel function of first kind and order n . This index is used to study the axisymmetric ($n=0$) or lateral ($n=1$) case, while m defines the circumferential symmetry of the problem. Axisymmetric primitive functions will be characterized by $n=m=0$, while lateral sloshing functions can be obtained with $n=m=1$.

However, the previous set of primitives does not satisfy Eq. (22e). The set of admissible functions is then created as a linear combination of the previous

$$\bar{\Phi}_i = \sum_{p=i}^{N+1} a_{ip} \vartheta_p, \quad \bar{\zeta}_i = \sum_{p=i}^{N+1} a_{ip} \zeta_p, \quad \bar{\xi}_i = \sum_{p=i}^{N+1} a_{ip} \xi_p, \quad (i=1, 2, \dots, N). \quad (33)$$

The $N+1-p$ coefficients a_{ip} for each i value are determined by imposing (i) a normalization condition, (ii) a contact angle value, and (iii) a Lagrange minimization problem designed to produce Bessel-like functions. These conditions are respectively expressed as [3]

$$\sum_{p=i}^{N+1} a_{ip} \zeta_p(1) = 1, \quad (34a)$$

$$\sum_{p=i}^{N+1} a_{ip} \zeta_{pR}(1) = \Gamma, \quad (34b)$$

$$\sum_{p=i}^{N+1} a_{ip}(K_{pj} - k_p^2 L_{pj}) + \lambda_{1i} \zeta_{jR}(1) + \lambda_{2i} \zeta_j(1) \quad (34c)$$

$$= 0 \quad (j=i, i+1, \dots, N, N+1),$$

where λ_{1i} and λ_{2i} are the Lagrange multipliers of the minimization problem and

$$\zeta_i(R) = \zeta_i(R, \theta) / \cos(m\theta), \quad (35)$$

$$K_{ij} = \iint_F \left(\zeta_{iR} \zeta_{jR} - \frac{n}{R^2} \zeta_i \zeta_j \right) R dR d\theta. \quad (36)$$

$$L_{ij} = \iint_F \zeta_i \zeta_j R dR d\theta. \quad (37)$$

Once the system is solved, the admissible set can be used to solve the eigenvalue problem.

The success of this method depends on finding an adequate set of admissible functions $\bar{\Phi}_i$ such that the eigenfunctions $\Phi^{(n)}$ can be represented with a reduced number of elements. The Z term in the primitives ϑ_p , evaluated at the equilibrium surface, grows exponentially when $F(R)$ departs significantly from $Z = 0$. This is the case of low Bond numbers and small contact angles. In [13] it is stated that for contact angles lower than 15° in the case of free-edge condition ($\Gamma = 0$) or lower than 60° for the stuck-edge condition ($\Gamma \rightarrow \infty$) the system may become numerically ill-conditioned. Furthermore, the comparison between this method and a finite differences approach showed significant divergences in the shape of the eigenfunctions $\Phi^{(n)}$ for particular cases.

A possible solution would be finding a set of primitive functions without exponential terms. To the best knowledge of the authors, and considering the attempts made in [3], an alternative has not yet been proposed. It should also be noted that the magnetic force generally flattens the equilibrium surface, hence mitigating the effect of the exponential term in Eq. (31a).

4 Case of Application

4.1 System description

CubeSats are a particular class of nanosatellites composed of standardized 10×10 cm cubic units (U) [47]. Their subsystems are designed to fit this standard, lowering the manufacturing costs and enhancing adaptability (e.g. the Aerojet MPS-130 propulsion module is offered in 1U or 2U formats). Due to the rapid decay of magnetic fields with distance, small spacecrafts with small propellant tanks may be particularly well suited for magnetic sloshing control implementations. Their development requires a dedicated feasibility study that is beyond the scope of this paper; however, the performance of an hypothetical system is here addressed.

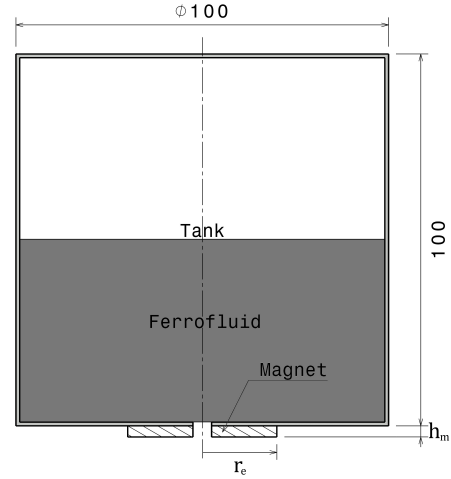


Fig. 2: Sketch of the case of application. Units in mm.

A 1U cylindrical container with 10 cm height, 5 cm radius and filled with a ferrofluid solution up to half of its height is subsequently considered. In order to generate a downward restoring force, a high-end cylindrical neodymium magnet magnetized at 1500 kA/m in the vertical direction is placed under the tank. The magnet has a hole of $r_i = 2.5$ mm radius at the center (liquid outlet), a height h_m , an external radius r_e and a density $\rho_m = 7010$ kg/m³. A contact angle of 67° is assumed in microgravity conditions. The sketch of this setup is given in Fig. 2.

The liquid is a 1:10 volume solution of the Ferrotec water-based EMG-700 ferrofluid with a 0.58% volume concentration of magnetic nanoparticles. Its magnetic properties were measured with a MicroSense EZ-9 Vibrating Sample Magnetometer at the Physics Department of Politecnico di Milano. The corresponding magnetization curve is depicted in Fig. 3 and shows an initial susceptibility $\chi = 0.181$ and saturation magnetization $M_s = 3160$ A/m. Viscosity is assumed to have a negligible effect on the free sloshing problem.

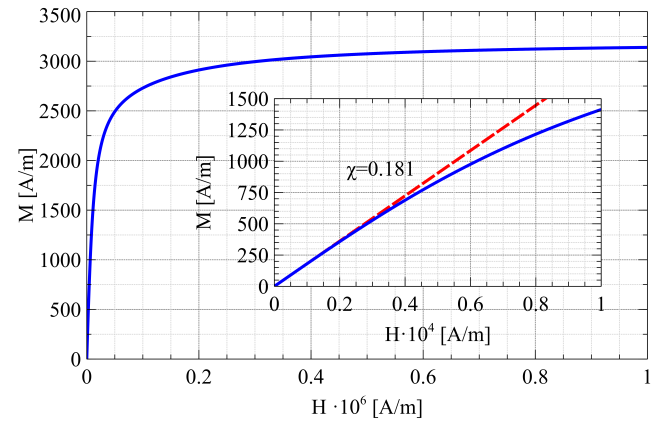


Fig. 3: Magnetization curve of the 1:10 solution of the Ferrotec EMG-700 water-based ferrofluid

4.2 Magnetic modeling

The magnetic system is modeled in Comsol Multiphysics, which is interfaced with the model developed in section 2. The FEM simulation is employed to estimate the fields \mathbf{H} and \mathbf{M} for a given magnet and equilibrium surface shape (meniscus). The last is computed iteratively by means of Eq. (12) with a FEM-in-the-loop implementation. Equation 21 is then employed to calculate the magnetic Bond number at the surface, that determines the solution of the free oscillation problem. The eigenfrequencies and eigenmodes of the system are finally obtained by solving Eq. (22).

To simulate the magnetic field, the model solves the stationary non-electric Maxwell equations

$$\nabla \times \mathbf{H} = 0, \quad (38)$$

$$\mathbf{B} = \nabla \times \mathbf{A}, \quad (39)$$

where \mathbf{A} is the magnetic vector potential produced by the magnetized materials. The constitutive relation

$$\mathbf{B} = \mu_0 (\mathbf{H} + \mathbf{M}) \quad (40)$$

is applied to the magnet with $\mathbf{M} = [0, 0, 1500]$ kA/m and to the surrounding air with $\mathbf{M} = \mathbf{0}$. The magnetization curve $M = f(H)$ given in Fig. 3 is applied to the ferrofluid volume.

The simulation domain is a rectangular 1×2 m region enclosing the container. An axisymmetric boundary condition is applied to the symmetry axis, while the tangential magnetic potential is imposed at the external faces through $\mathbf{n} \times \mathbf{A} = \mathbf{n} \times \mathbf{A}_0$. \mathbf{A}_0 is the dipole term of the magnetic vector potential generated by the magnetization fields of the magnet and ferrofluid. Consequently, \mathbf{A}_0 is computed as the potential vector generated by two point dipoles applied at the

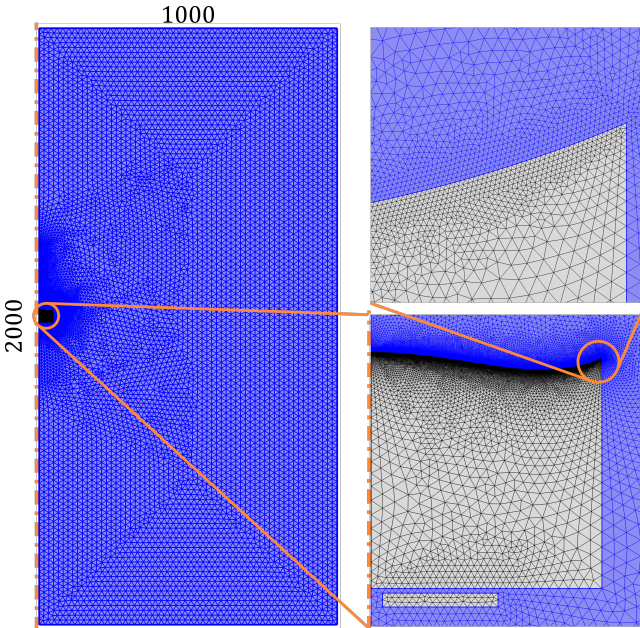


Fig. 4: Mesh and overall dimensions of the magnetic FEM simulation domain. Units in mm.

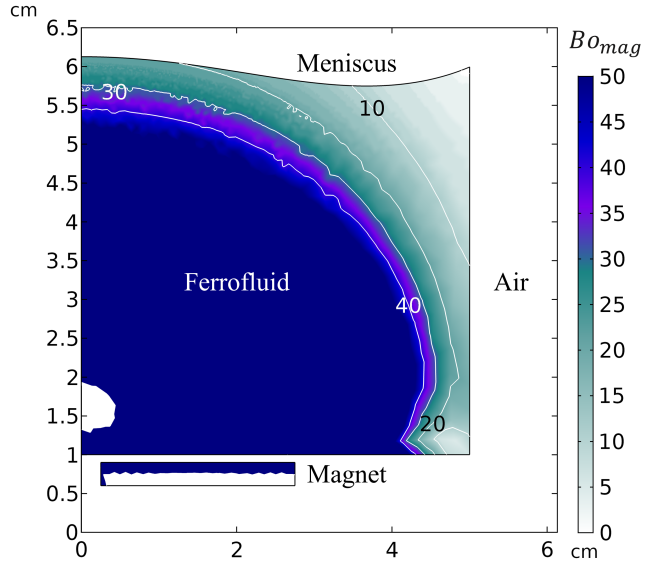


Fig. 5: Equilibrium configuration of the magnetic sloshing damping system for $h_m = 5$ mm and $r_e = 2.8$ cm. The magnetic Bond number is represented in the color scale for the range of interest.

centers of the magnetization distributions and whose dipole moments are those of said distributions. While the dipole associated to the magnet can be calculated beforehand, the ferrofluid dipole needs to be approximated iteratively by integrating \mathbf{M} in the ferrofluid volume. The relative error in the magnetic vector potential due the dipole approximation is estimated to be below 0.03% at the boundary of the domain with respect to the exact value generated by the equivalent circular loop.

The mesh is composed by 53000 irregular triangular elements and is refined at the meniscus, as shown in Fig. 4. Mean and minimum condition numbers of 0.983 and 0.766 are measured.

Figure 5 shows a particular configuration of analysis. Positive and negative curvatures are observed at the meniscus due to the high intensity of the magnetic field. Weaker magnets would result in convex equilibrium surfaces, as in the non-magnetic case. It should be noted that the magnetic Bond number rapidly decreases with distance to the source, spanning between 0 and 20 at the free surface.

4.3 Parametric analysis

Figure 6 depicts the fundamental sloshing frequency ω_1 , corresponding to the lowest root of Eq. (29), as a function of the external radius r_e and height h_m of the magnet. $N = 7$ admissible functions were employed in the computation. The mass of the magnet is given in a second scale, reflecting the technical trade-off between mass and sloshing frequency. Larger magnets result in stronger restoring forces and higher sloshing frequencies. For example, a downward 7 N force and a 100% increase in the fundamental sloshing frequency would be achieved with a 3 mm height, 30 mm external ra-

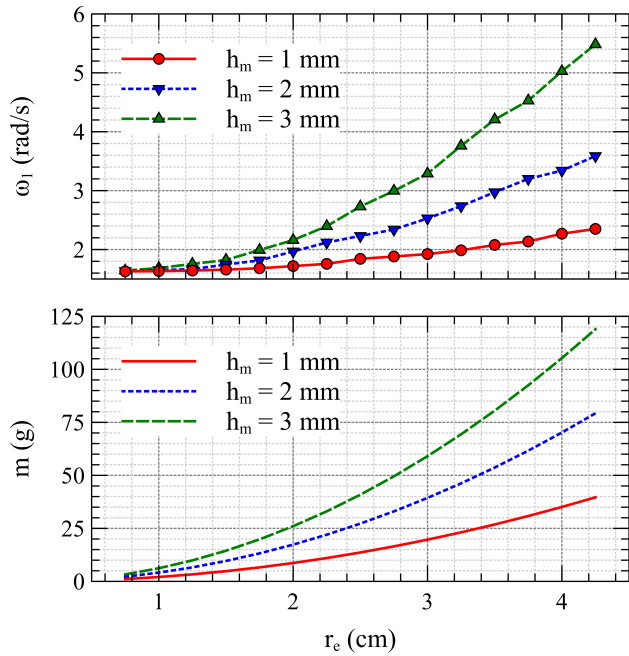


Fig. 6: Fundamental sloshing frequency ω_1 (top) and mass of the magnet (bottom) as a function of the height h_m and external radius r_e of the magnet

dius and 60 grams magnet. Unlike the non-magnetic case, the presence of a significant restoring force ensures that the assumption of small oscillations (linear sloshing) is not violated for moderate displacements of the container.

A small fluctuation in the frequency plot appears due to numerical errors. The procedures for solving Eq. (12) are highly dependent on the initial estimation of λ . This behavior has been extensively reported in the bibliography [3, 24]

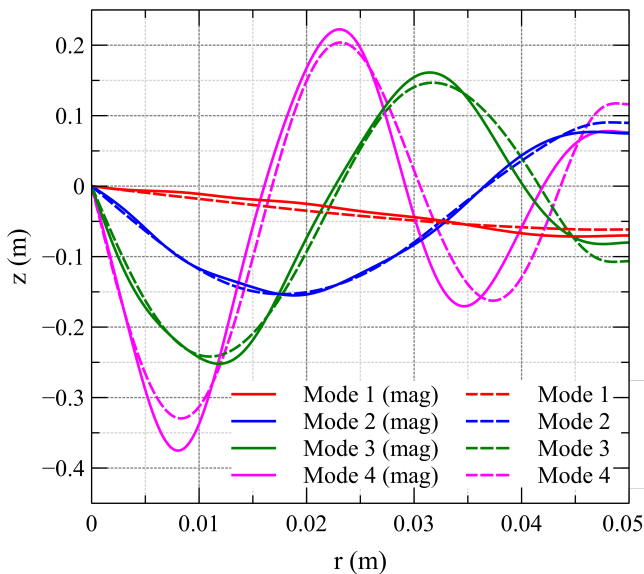


Fig. 7: Magnetic and non-magnetic sloshing modes shape for the case under analysis

and is further complicated by the magnetic interaction. In addition, the eigenvalue problem that provides the natural frequencies of the system becomes ill-conditioned if the actual modal shapes diverge significantly from the primitive functions [13]. For strong magnetic fields, this may certainly be the case. The problem would be solved if a finite differences approach is employed instead of Ritz's method.

The modal shapes for the 3 mm height and 30 mm external radius magnet are represented in Fig. 7 together with the non-magnetic modes (i.e. the ones obtained when the magnet is removed). Although the profiles are essentially the same, it is interesting to observe how the fundamental mode slightly reduces and increases its displacement where the magnetic Bond number is greater and smaller, respectively. This is consistent with the aforementioned stabilizing role of the magnetic force.

5 Conclusions

A quasi-analytical model has been developed to study the sloshing of magnetic liquids in low-gravity conditions. The magnetic interaction modifies the shape of the meniscus and the effective inertial acceleration of the system as shown in Eq. (13) and Eq. (17), respectively. As a consequence, a shift of the eigenfrequencies and a modification of the eigenmodes of the free oscillations problem is produced. The framework here presented extends the models developed in previous works [3, 12] by adding the magnetic and axisymmetric cases.

The small oscillations assumption is generally not valid for non-magnetic sloshing in microgravity, which is usually characterized by complex non-linear deformations driven by surface tension. In the magnetic case, however, the linear treatment of the problem is endorsed by a significant magnetic restoring force. It would be reasonable to ask how strong magnetic fields affect the shape of the eigenmodes and hence the reliability of Ritz's approximation. Since this procedure has been historically discussed [13], the computation of a finite-differences-based solution becomes particularly convenient for future implementations. Ritz's method represents, however, the simplest tool to solve the variational formulation given by Eq. (22) and has been presented for illustrative purposes.

From the engineering viewpoint, the magnetic sloshing concept represents an opportunity to develop new sloshing control devices for microsatellites. Unlike the non-magnetic case, the response of the system can be easily predicted, quantified and simulated by means of mechanical analogies. These simplified models can be easily embedded in a controller (e.g. a linear observer) used to predict and compensate the sloshing disturbances of a spacecraft in orbit. The spacecraft would then benefit from a significantly improved pointing performance.

Acknowledgements

The authors thank their institutions, Politecnico di Milano and the University of Seville, for their financial and

academic support. The discussions with Prof. Miguel Ángel Herrada Gutiérrez on the verification of the non-magnetic model were highly appreciated.

References

- [1] Reynolds, W. C., and Satterlee, H. M., 1966. “The dynamic behavior of liquids in moving containers, ch. 11”. *NASA Technical Report*, **SP-106**.
- [2] Eswaran, M., and Saha, U. K., 2011. “Sloshing of liquids in partially filled tanks - a review of experimental investigations”. *Ocean Systems Engineering*, **1**(2), pp. 131–155.
- [3] Satterlee, H. M., and Reynolds, W. C., 1964. “The dynamics of free liquid surface in cylindrical containers under strong capillary and weak gravity conditions”. *Stanford University Mechanical Engineering Department*, **LG-2**.
- [4] Dodge, F. T., and Garza, L. R., 1969. “Experimental and theoretical studies of liquid sloshing at simulated low gravities”. *NASA Technical Report*, **CR-80471**.
- [5] Concus, P., Crane, G., and Satterlee, H., 1967. “Small amplitude lateral sloshing in a cylindrical tank with a hemispherical bottom under low gravitational conditions”. *NASA Technical Report*, **CR-54700**.
- [6] Concus, P., Crane, G., and Satterlee, H., 1969. “Small amplitude lateral sloshing in spheroidal containers under low gravitational conditions”. *NASA Technical Report*, **CR-72500**.
- [7] Salzman, J. A., and Masica, W. J., 1969. “Lateral sloshing in cylinders under low-gravity conditions”. *NASA Technical Report*, **TN D-5058**.
- [8] Dodge, F. T., and Garza, L. R., 1970. “Simulated low-gravity sloshing in spherical, ellipsoidal, and cylindrical tanks”. *Journal of Spacecraft and Rockets*, **7**(2), pp. 204–206.
- [9] Bauer, H. F., and Eidel, W., 1990. “Linear liquid oscillations in cylindrical container under zero-gravity”. *Applied Microgravity Technology*, **2**, pp. 212–220.
- [10] Dodge, F. T., 1971. “Further studies of propellant sloshing under low-gravity conditions”. *NASA Technical Report*, **CR-119892**.
- [11] Coney, T., and Salzman, J., 1971. “Lateral sloshing in oblate spheroidal tanks under reduced- and normal-gravity conditions”. *NASA Technical Report*, **TN D-6250**.
- [12] Yeh, G. C. K., 1967. “Free and forced oscillations of a liquid in an axisymmetric tank at low-gravity environments”. *Journal of Applied Mechanics*, **34**(1), pp. 23–28.
- [13] Concus, P., and Crane, G. E., 1967. “Discussion: Free and forced oscillations of a liquid in an axisymmetric tank at low-gravity environments”. *Journal of Applied Mechanics*, **34**(4), pp. 1051–1052.
- [14] Chu, W.-H., 1970. “Low-gravity fuel sloshing in an arbitrary axisymmetric rigid tank”. *Journal of Applied Mechanics*, **37**(3), pp. 828–837.
- [15] Myshkis, A., and Wadhwa, R., 1987. *Low-gravity fluid mechanics: mathematical theory of capillary phenomena*. Springer.
- [16] Hung, R. J., Lee, C. C., and Leslie, F. W., 1992. “Similarity rules in gravity jitterrelated spacecraft liquid propellant slosh waves excitation”. *Journal of Fluids and Structures*, **6**(4), pp. 493–522.
- [17] Snyder, H., 1999. “Sloshing in microgravity”. *Cryogenics*, **39**(12), pp. 1047 – 1055.
- [18] Peterson, L. D., Crawley, E. F., and Hansman, R. J., 1989. “Nonlinear fluid slosh coupled to the dynamics of a spacecraft”. *AIAA Journal*, **27**(9), pp. 1230–1240.
- [19] Luppés, R., Helder, J. A., and Veldman, A. E., 2006. “The numerical simulation of liquid sloshing in microgravity”. In *Computational Fluid Dynamics 2006*, H. Deconinck and E. Dick, eds., Springer, Berlin, Heidelberg, pp. 607–612.
- [20] Utsumi, M., 1988. “Liquid sloshing in an axisymmetric container in low-gravity environments”. In *16th International Symposium on Space Technology and Science*, Vol. 1, pp. 815–826.
- [21] Utsumi, M., 1990. “The meniscus and sloshing of a liquid in an axisymmetric container at low-gravity”. *JSMIE international journal. Ser. 3, Vibration, control engineering, engineering for industry*, **33**(3), pp. 346–356.
- [22] Utsumi, M., 1998. “Low-gravity propellant slosh analysis using spherical coordinates”. *Journal of Fluids and Structures*, **12**(1), pp. 57 – 83.
- [23] Utsumi, M., 2004. “A mechanical model for low-gravity sloshing in an axisymmetric tank”. *Journal of Applied Mechanics*, **71**(5), pp. 724–730.
- [24] Dodge, F., 2000. *The New Dynamic Behavior of Liquids in Moving Containers*. Southwest Research Institute.
- [25] Chipchark, D., 1963. “Development of expulsion and orientation systems for advanced liquid rocket propulsion systems”. *USAF Technical Report*(RTD-TDR-63-1048).
- [26] Ramachandran, N., Leslie, F., Peters, P., and Sisk, R., 1998. “A novel method of gradient forming and fluid manipulation in reduced gravity environments”. In *36th AIAA Aerospace Sciences Meeting and Exhibit*, AIAA, ed.
- [27] Marchetta, J. G., and Winter, A. P., 2010. “Simulation of magnetic positive positioning for space based fluid management systems”. *Mathematical and Computer Modelling*, **51**(9), pp. 1202 – 1212.
- [28] Papell, S., 1963. “Low viscosity magnetic fluid obtained by the colloidal suspension of magnetic particles”. *US Patent*, **3215572**.
- [29] Neuringer, J. L., and Rosensweig, R. E., 1964. “Ferrohydrodynamics”. *The Physics of Fluids*, **7**(12), pp. 1927–1937.
- [30] Rosensweig, R., 1997. *Ferrohydrodynamics*. Dover Publications.
- [31] Martin, J., and Holt, J., 2000. “Magnetically actuated propellant orientation experiment, controlling fluid motion with magnetic fields in a low-gravity environment”. *NASA Technical Report*, **TM-2000-210129**.

- [32] Marchetta, J., and Hochstein, J., 1999. “Fluid capture by a permanent ring magnet in reduced gravity”. In 37th Aerospace Sciences Meeting and Exhibit, AIAA.
- [33] Marchetta, J., and Hochstein, J., 2000. “Simulation and dimensionless modeling of magnetically induced reorientation”. In 38th Aerospace Sciences Meeting and Exhibit, AIAA.
- [34] Marchetta, J., Hochstein, J., Sauter, D., and Simmons, B., 2002. “Modeling and prediction of magnetic storage and reorientation of lox in reduced gravity”. In 40th AIAA Aerospace Sciences Meeting and Exhibit, AIAA.
- [35] Ohno, K., Shimoda, M., and Sawada, T., 2008. “Optimal design of a tuned liquid damper using a magnetic fluid with one electromagnet”. *Journal of Physics: Condensed Matter*, **20**(20), p. 204146.
- [36] Ohno, K., Suzuki, H., and Sawada, T., 2011. “Analysis of liquid sloshing of a tuned magnetic fluid damper for single and coaxial cylindrical containers”. *Journal of Magnetism and Magnetic Materials*, **323**(10), pp. 1389 – 1393.
- [37] Ohaba, M., and Sudo, S., 1995. “Liquid surface behavior of a magnetic liquid in a container subjected to magnetic field and vertical vibration”. *Journal of Magnetism and Magnetic Material*, **149**, pp. 38–41.
- [38] Sudo, S., Nishiyama, H., Katagiri, K., and Tani, J., 1999. “Interactions of magnetic field and the magnetic fluid surface”. *Journal of Intelligent Material Systems and Structures*, **10**(6), pp. 498–504.
- [39] Kaneko, S., Ishiyama, T., and Sawada, T., 2013. “Effect of an applied magnetic field on sloshing pressure in a magnetic fluid”. *Journal of Physics: Conference Series*, **412**(1), p. 012018.
- [40] Ishiyama, T., Kaneko, S., Takemoto, S., and Sawada, T., 2014. “Relation between dynamic pressure and displacement of free surface in two-layer sloshing between a magnetic fluid and silicone oil”. In Applied Electromagnetic Engineering for Magnetic, Superconducting, Multifunctional and Nano Materials, Vol. 792 of *Materials Science Forum*, Trans Tech Publications, pp. 33–38.
- [41] Sawada, T., Ohira, Y., and Houda, H., 2002. “Sloshing motion of a magnetic fluid in a cylindrical container due to horizontal oscillation”. *Energy Conversion and Management*, **43**(3), pp. 299–308.
- [42] Dodge, F. T., and Garza, L. R., 1972. “Free-surface vibrations of a magnetic liquid”. *Journal of Engineering for Industry*, **94**(1), pp. 103–108.
- [43] Lamb, H., 1895. *Hydrodynamics*. University Press.
- [44] Sawada, T., Kikura, H., and Tanahashi, T., 1999. “Kinematic characteristics of magnetic fluid sloshing in a rectangular container subject to non-uniform magnetic fields”. *Experiments in Fluids*, **26**(3), pp. 215–221.
- [45] Hildebrand, F., 1965. *Methods of applied mathematics*. Prentice-Hall.
- [46] Dodge, F., and Garza, L., 1967. “Experimental and theoretical studies of liquid sloshing at simulated low gravity”. *Journal of Applied Mechanics*, **34**(3), pp. 555–562.
- [47] Heidt, H., Puig-Suari, J., Moore, A. S., Nakasuka, S., and Twiggs, R. J. “Cubesat: A new generation of picosatellite for education and industry low-cost space experimentation”. In Proceedings of the AIAA/USU Conference on Small Satellites.

List of Figures

| | | |
|---|---|----|
| 1 | Geometry of the system under analysis, composed by a magnetic liquid that fills a container in microgravity while subjected to an external magnetic field. S' and C' refer to the meniscus surface and contour, while S and C are the dynamic fluid surface and contour, respectively. O denotes the vertex of the meniscus, W is the vessel wall and V denotes the fluid volume. | 3 |
| 2 | Sketch of the case of application. Units in mm. | 8 |
| 3 | Magnetization curve of the 1:10 solution of the Ferrotec EMG-700 water-based ferrofluid | 8 |
| 4 | Mesh and overall dimensions of the magnetic FEM simulation domain. Units in mm. . | 9 |
| 5 | Equilibrium configuration of the magnetic sloshing damping system for $h_m = 5$ mm and $r_e = 2.8$ cm. The magnetic Bond number is represented in the color scale for the range of interest. | 9 |
| 6 | Fundamental sloshing frequency ω_1 (top) and mass of the magnet (bottom) as a function of the height h_m and external radius r_e of the magnet | 10 |
| 7 | Magnetic and non-magnetic sloshing modes shape for the case under analysis | 10 |